

# Emergence of correlation-driven altermagnetism in Hubbard model on geometrically frustrated square lattice

Md Fahad Equbal \* and M. A. H. Ahsan †

*Department of Physics, Jamia Millia Islamia (Central University), New Delhi 110025, India*

(Dated: March 3, 2026)

We investigate the emergence of altermagnetism—a collinear magnetic phase characterized by large non-relativistic spin splitting and zero net magnetization—driven by electronic correlations on  $3 \times 3$  geometrically frustrated square lattice. Using exact diagonalization of the simple and the extended Hubbard model, we analyze the interplay between on-site repulsion  $U$ , nearest-neighbor (NN) Coulomb interaction  $V$  and geometric frustration across various filling factors ( $N = 8, 9, 10$ ). Unlike traditional models that rely on single-particle anisotropy or specific sublattice geometries, our results demonstrate that altermagnetic signatures arise from many-body fluctuations in doped Mott insulators. We find that while geometric frustration suppresses altermagnetism at half-filling ( $N = 9$ ), carrier doping (hole ( $N = 8$ ) or electron ( $N = 10$ )) stabilizes robust, rotationally symmetric altermagnetic correlations. Furthermore, we identify a critical threshold for the NN interaction  $V$  at intermediate coupling ( $U = 4$ ) where the altermagnetic state in the electron-doped sector undergoes a first-order-like transition, whereas strong coupling ( $U = 10$ ) stabilizes well-formed local moments and preserves the anisotropic spin texture. This work establishes a fluctuation-mediated route to altermagnetism on symmetric geometrically frustrated lattices and identifies carrier concentration and the NN Coulomb interaction as a critical tunable parameter for controlling magnetic anisotropy in strongly correlated systems.

**Keywords:** Altermagnetism; Electronic correlations; Geometric frustration; Hubbard model; Exact diagonalization

## I. INTRODUCTION

Strongly correlated electron systems remain at the forefront of condensed matter physics due to the rich interplay between charge, spin and lattice degrees of freedom [1, 2] that gives rise to emergent quantum phases such as Mott insulators [3–6], unconventional superconductors [7–10], quantum spin liquids [11–13] and exotic magnetic states [14–18]. The Hubbard model [19–21] and its extensions [22] provide the minimal microscopic framework for capturing these phenomena, interpolating between itinerant and localized regimes through the competition between kinetic energy, on-site Coulomb repulsion and non-local interactions. In the strong-coupling limit, the model maps onto effective Heisenberg-type spin Hamiltonians [23, 24], while at intermediate coupling it retains simultaneous charge and spin fluctuations, making it particularly sensitive to carrier dopings (hole or electron) and geometric frustration [25, 26].

Recent years have witnessed growing interest in altermagnetism, a class of collinear magnets that break spin degeneracy in momentum space despite vanishing net magnetization and preserved combined symmetries distinct from conventional ferromagnets and antiferromagnets [27–30]. Unlike conventional antiferromagnets, where spin-degenerate bands are protected by combined time-reversal and translation or inversion symmetries [31], altermagnets display momentum-dependent spin splitting analogous to  $d$ -,  $g$ - or  $i$ -wave pairing symmetries [32–34]. This unique combination of properties positions altermagnets as promising platforms for next-generation spintronic devices, including terahertz oscillators, spin-torque elements and topolog-

ical quantum applications [35–40]. The identification of altermagnetic signatures in correlated systems has opened new perspectives on how electron-electron interactions can generate symmetry-selective spin responses even in centrosymmetric lattices [41–44].

From a microscopic viewpoint, the emergence of altermagnetic correlations is intimately connected to the interplay between local moment formation and spatial organization of spin correlations [45, 46]. Geometric frustration plays a pivotal role in suppressing conventional long-range magnetic order and promoting unconventional correlated states [47]. On frustrated lattices, competing exchange pathways prevent simple bipartite Néel ordering, often stabilizing highly degenerate manifolds [48, 49], spin-liquid-like correlations [50, 51] or spatially modulated spin textures [52].

In this work, we investigate the simple and the extended Hubbard model using exact diagonalization (ED) [53, 54] on the frustrated  $3 \times 3$  square lattice with periodic boundary conditions (PBC) as shown in Fig. 1. This minimal toroidal geometry retains full quantum coherence while incorporating geometric frustration and non-trivial loop connectivity. By systematically analyzing half-filling and single-carrier (hole or electron) doped sectors ( $N = 8, 9, 10$ ), where  $N$  represents number of electrons, we isolate how carrier itinerancy modifies local moment formation, altermagnetic correlations and rotational symmetry properties across intermediate ( $U = 4$ ) and strong-coupling ( $U = 10$ ) regimes.

The choice of a frustrated  $3 \times 3$  square lattice is deliberate. Unlike larger bipartite lattices that trivially support Néel order, this minimal geometry suppresses classical ordering tendencies and enhances sensitivity to symmetry-selective spin responses. It therefore serves as a controlled platform for identifying whether altermagnetic correlations are intrinsic electronic phenomena or artifacts of spontaneous symmetry breaking.

The remainder of this manuscript is organized as follows.

\* md179654@st.jmi.ac.in

† mahsan@jmi.ac.in

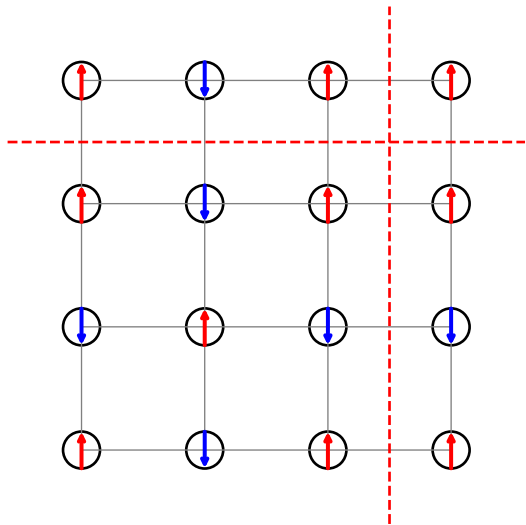


FIG. 1. Schematic representation of the frustrated square lattice with periodic boundary conditions. The red dashed lines mark the periodic wrapping in both spatial directions.

In Sec. II we introduce the model Hamiltonian and discuss the formalism to study correlation-driven altermagnetism, including the definition of our key diagnostics. Section III presents our results, beginning with the simple Hubbard model ( $V = 0$ ) to establish the role of doping and frustration, followed by a detailed analysis of the extended Hubbard model at intermediate ( $U = 4$ ) and strong ( $U = 10$ ) coupling. Finally, in Sec. IV we provide a summary and conclusion of this work.

## II. MODEL AND METHOD

We investigate the phenomenon of altermagnetism in the simple and the extended Hubbard model on frustrated square lattice of size  $3 \times 3$  with periodic boundary conditions (PBC) in both spatial directions (torus geometry). The one-band extended Hubbard Hamiltonian is written as [22]

$$H = -t \sum_{\langle ij \rangle \sigma} (c_{i\sigma}^\dagger c_{j\sigma} + h.c.) + U \sum_i n_{i\uparrow} n_{i\downarrow} + V \sum_{\langle ij \rangle} n_i n_j, \quad (1)$$

where  $i$  and  $j$  stands for the sites of square lattice with  $\langle ij \rangle$  representing summation over ordered pairs of NN only. Operator  $c_{i\sigma}^\dagger$  ( $c_{i\sigma}$ ) creates (annihilates) an electron with spin  $\sigma \in \{\uparrow, \downarrow\}$  on site  $i$ ,  $n_{i\sigma} = c_{i\sigma}^\dagger c_{i\sigma}$  is the fermion number operator,  $n_i = n_{i\uparrow} + n_{i\downarrow}$  and  $h.c.$  means Hermitian conjugate. Parameters  $t$ ,  $U$  and  $V$  represents the NN hopping matrix amplitude, the on-site Coulomb interaction and the NN Coulomb interaction respectively. In the  $V = 0$  limit, Eq. 1 reduces to the simple Hubbard model. In the non-interacting ( $U = V = 0$ ) case, the Hamiltonian  $H$  with NN hopping has dispersion relation given by  $\epsilon_k = -2t(\cos k_x + \cos k_y)$  with bandwidth  $W = 8t$  for 2D systems in the thermodynamic limit. On the  $3 \times 3$  torus, however, the combination of PBC and odd number of site frustrates simple bipartite Néel order. This geometric frustration plays a central role in giving rise to unconventional

spin-spin correlation and is a key ingredient in the present study of altermagnetism.

We consider the  $3 \times 3$  geometrically frustrated square lattice at half-filling ( $N = 9$ ) and with one-hole ( $N = 8$ ) and one-electron ( $N = 10$ ) doping. For each filling, calculations are restricted to the lowest total-spin sector i.e.,  $S = \frac{1}{2}$  for  $N = 9$  and  $S = 0$  for  $N = 8, 10$ , thereby focusing on magnetically compensated states dominated by quantum fluctuations.

The Hamiltonian is diagonalized using exact diagonalization (ED) in spin-adapted basis [55, 56] that explicitly resolves the total-spin quantum number  $S$ . Exploiting the full  $SU(2)$  spin-rotation symmetry of the model,  $[H, S^2] = [H, S^z] = 0$ , the Hilbert space breaks up into independent spin sectors. This approach provides two decisive advantages: (i) a significant reduction in the Hilbert space dimensionality, and (ii) direct access to distinct spin sectors, allowing us to analyze interaction-driven reorganization of spin correlation. For each set of parameters ( $U, V$ ), we compute the ground-state and a few low-lying excited states, from which equal-time correlation functions are evaluated without mean-field decoupling or uncontrolled approximations.

To diagnose altermagnetic correlations beyond conventional magnetic order, we introduce a site-resolved altermagnetic correlation matrix constructed from equal-time spin-spin correlation

$$\Omega_{ij} = \langle \mathbf{S}_i \cdot \mathbf{S}_j \rangle \eta_{ij} \mathcal{C}_i, \quad (2)$$

where  $\mathbf{S}_{i(j)}$  denotes the spin operator at site  $i(j)$ . The factor  $\eta_{ij} = \pm 1$  is a real-space staggered sign structure reflecting altermagnetic symmetry and  $\mathcal{C}_i = 1 - 2|\langle n_{i\uparrow} \rangle - \langle n_{i\downarrow} \rangle|$  is a local compensation factor that suppresses trivial spin-polarized contributions with  $\langle n_{i\sigma} \rangle$  denoting the spin-resolved local density. Both  $\langle \mathbf{S}_i \cdot \mathbf{S}_j \rangle$  and  $\mathcal{C}_i$  are strictly invariant under time reversal.  $\Omega_{ij}$  reorganizes the spin-spin correlation matrix in a manner that isolates compensated, anisotropic spin correlation generated by electronic interactions and geometric frustration. In the lowest-spin sector considered in this work,  $\mathcal{C}_i \approx 1$ , ensuring that the observed signals originate from strong electronic correlations rather than residual local spin polarization.

On finite-size lattice, ED lacks a well-defined spin-resolved band dispersions  $E_{k\sigma}$ . Hence, we quantify altermagnetic tendencies through symmetry-projected real-space correlations and define the site-resolved altermagnetic spin-response measure as

$$\Delta_i^{\text{spin}} = \frac{1}{N_b(i)} \sum_j \Omega_{ij}, \quad (3)$$

where  $N_b(i)$  is the number of bonds connected to site  $i$ . To characterize the global altermagnetic response, we define the average spin-response measure

$$\langle \Delta_{\text{spin}} \rangle = \frac{1}{M} \sum_i \Delta_i^{\text{spin}}, \quad (4)$$

where  $M$  is the total number of lattice sites. Although defined entirely in real space,  $\langle \Delta_{\text{spin}} \rangle$  serves as a diagnostic measure of altermagnetic correlations by selectively amplifying staggered, anisotropic spin-correlation patterns that

are suppressed in isotropic antiferromagnetic or ferromagnetic states.

While  $\langle \Delta_{\text{spin}} \rangle$  identifies the spatial organization of spins, it does not inherently distinguish between changes in the spatial correlation structure and changes in the magnitude of the spins themselves. To decouple the effects of magnetic order from the local physics of electron correlation, we examine the average local moment defined as

$$\bar{m} = \frac{4}{N} \sum_i \langle (n_{i\uparrow} - n_{i\downarrow})^2 \rangle \quad (5)$$

which quantifies the degree of electron localization and the strength of the local magnetic polarization.

To further quantify directional differentiation of these correlations, we introduce the anisotropy parameter

$$\mathcal{A} = \frac{1}{M} \sum_i |\Delta_i^x - \Delta_i^y|, \quad (6)$$

where  $\Delta_i^{x(y)}$  is obtained by restricting the sum in Eq. 3 to bonds oriented along the  $x(y)$  lattice direction. A finite value of  $\mathcal{A}$  indicates direction-dependent anisotropy in the altermagnetic spin correlation induced by geometric frustration and electronic interactions.

### III. RESULTS AND DISCUSSION

We now present and discuss our results of the correlation-driven altermagnetic responses on the geometrically frustrated  $3 \times 3$  square lattice. We begin with the simple Hubbard model ( $V = 0$ ), examining the interplay between on-site interaction and geometric frustration. We then investigate how the inclusion of NN Coulomb interaction affect these trends within the extended Hubbard model.

#### A. Simple Hubbard Model ( $V = 0$ )

To quantify the emergence of altermagnetic tendencies on the geometrically frustrated square lattice, in Fig. 2 we analyze the evolution of the average spin-response measure  $\langle \Delta_{\text{spin}} \rangle$ , as a function of the on-site Coulomb interaction  $U$  for half-filling ( $N = 9, S = \frac{1}{2}$ ) and for one-hole ( $N = 8, S = 0$ ) and one-electron ( $N = 10, S = 0$ ) doping. At half-filling,  $\langle \Delta_{\text{spin}} \rangle$  decays monotonically with increasing interaction strength  $U$ . In the strong-coupling limit ( $U \gg t$ ),  $\langle \Delta_{\text{spin}} \rangle$  approaches zero, indicating that while local moments are well-formed, they fail to organize into the specific staggered, anisotropic patterns required for altermagnetism. This suppression arises from geometric frustration, which prevents bipartite Néel ordering and instead gives rise to a manifold of nearly degenerate, disordered spin configurations, leading to spin-liquid-like fluctuations. In contrast, the doped systems ( $N = 8$  and  $N = 10$ , both with total-spin  $S = 0$ ) exhibit a robust enhancement of altermagnetic correlations with increasing  $U$ . For the one-electron doped case ( $N = 10$ ), we observe a sharp rise in  $\langle \Delta_{\text{spin}} \rangle$ , which eventually saturates in the large- $U$  limit. The one-hole-doped case ( $N = 8$ ) follows a qualitatively

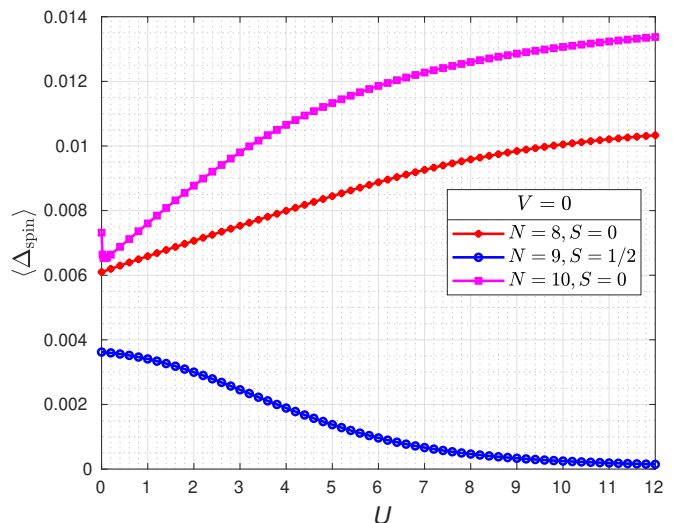


FIG. 2. Average altermagnetic spin-response measure  $\langle \Delta_{\text{spin}} \rangle$  as a function of on-site interaction  $U$  for the simple Hubbard model on  $3 \times 3$  frustrated square lattice. Results are shown for half-filling ( $N = 9, S = \frac{1}{2}$ ) and for one-hole ( $N = 8, S = 0$ ) and one-electron ( $N = 10, S = 0$ ) doping.

similar trend but with a consistently lower magnitude. The emergence of strong altermagnetic correlations in the  $S = 0$  sector points to a doping-induced mechanism. While geometric frustration prevents long-range order at half-filling, introducing a mobile charge carrier (hole or electron) allows the system to lower its kinetic energy by preferentially selecting specific anisotropic hopping paths. Through the interaction  $U$ , this kinetic energy scale couples to the spin degrees of freedom, stabilizing the staggered, compensated spin pattern captured by  $\langle \Delta_{\text{spin}} \rangle$ . The stronger response for electron doping ( $N = 10$ ) reveals a distinct particle-hole asymmetry in the altermagnetic susceptibility, likely a consequence of the underlying lattice dispersion and its interplay with geometric frustration.

To further elucidate the nature of the magnetic states, we examine the average local moment  $\bar{m}$  as a function of  $U$ , shown in Fig. 3. For all fillings considered ( $N = 8, 9, 10$ ),  $\bar{m}$  increases monotonically with  $U$ . This reflects a universal crossover from a weakly correlated metallic regime to a regime of well-defined local moments as the energetic cost for double occupancy increases. At half-filling ( $N = 9$ ),  $\bar{m}$  approaches its theoretical maximum most rapidly, indicating a robust Mott-insulating state with one electron localized per site. The comparison between  $\bar{m}$  and  $\langle \Delta_{\text{spin}} \rangle$  reveals a key distinction between local moment formation and altermagnetic correlations. At half-filling, the system exhibits the strongest local moments  $\bar{m}$ , yet the altermagnetic response  $\langle \Delta_{\text{spin}} \rangle$  is minimal. This demonstrates that the suppression of altermagnetism at half-filling does not arise from an absence of magnetism, but rather from the inability of frustrated local moments to organize into the specific anisotropic, staggered correlation patterns that characterize the altermagnetic phase. In contrast, in the doped  $S = 0$  sectors, the growth of local moments is accompanied by a strong enhancement of the altermagnetic response. The presence of mobile carriers enables kinetic energy exchange

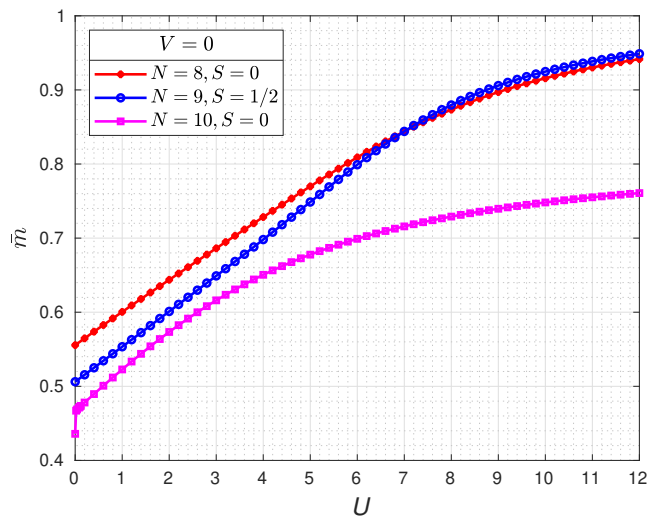


FIG. 3. Average local moment  $\bar{m}$  as a function of on-site interaction  $U$  for the simple Hubbard model on  $3 \times 3$  frustrated square lattice. Results are shown for half-filling ( $N = 9$ ,  $S = \frac{1}{2}$ ) and for one-hole ( $N = 8$ ,  $S = 0$ ) and one-electron ( $N = 10$ ,  $S = 0$ ) doping.

that couples localized spins anisotropically, thereby selecting correlation patterns consistent with altermagnetic symmetry. Notably, although the hole-doped system exhibits slightly larger local moments than the electron-doped case at large  $U$ , its altermagnetic response remains weaker. This reveals that altermagnetism is not determined by the magnitude of local moments alone, but instead depends sensitively on the coupling of those moments through charge dynamics.

To resolve the spatial structure of the interaction-induced magnetic states, we examine the site-resolved altermagnetic correlation matrix,  $\Omega_{5j}$ . This quantity characterizes the correlation between the central reference site (site 5) and all other sites  $j$  on the  $3 \times 3$  lattice. The resulting heatmaps, shown in Fig. 4, provide a direct real-space visualization of how geometric frustration and carrier doping control the spatial organization of compensated spin correlations.

At half-filling (middle row, Fig. 4), the system exhibits a weak and fragmented correlation pattern, lacking a coherent staggered structure. This confirms that geometric frustration on the  $3 \times 3$  lattice prevents the formation of altermagnetic order at half-filling. Despite the presence of well-formed local moments, the spatial correlations remain disordered, resulting in the small  $\langle \Delta_{\text{spin}} \rangle$  observed in Fig. 2. In contrast, the doped systems exhibit highly structured and anisotropic correlation patterns with increasing  $U$ . In the one-hole-doped system (top row, Fig. 4), the central site shows strong positive self-correlation, while correlations with its NN along the cardinal axes display distinct variations in both magnitude and sign. The one-electron-doped system (bottom row, Fig. 4) develops an even more pronounced staggered pattern. At strong coupling ( $U = 12$ ), the matrix elements  $\Omega_{5j}$  clearly distinguish between  $x$ - and  $y$ -directed bonds, forming a pattern consistent with  $d$ -wave symmetry. The spatial heatmaps thus provide microscopic confirmation of the trends observed in  $\langle \Delta_{\text{spin}} \rangle$ .

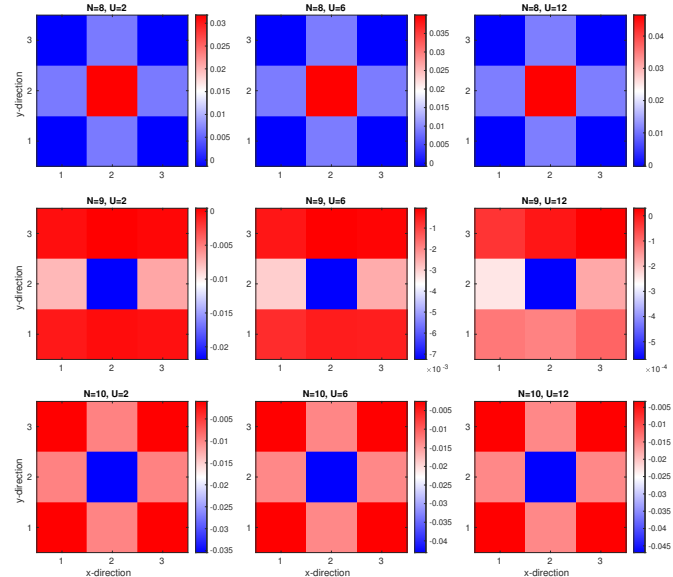


FIG. 4. Real-space heatmaps of the altermagnetic correlation matrix element  $\Omega_{5j}$  for the central reference site (site 5) on the  $3 \times 3$  frustrated square lattice at  $U = 2, 6, 12$ . Results are shown for  $N = 8$  (top-row),  $N = 9$  (middle-row) and  $N = 10$  (bottom-row). Doped sectors exhibit pronounced, interaction-enhanced anisotropic correlation patterns, whereas the half-filled case shows strongly suppressed and nearly uniform correlations due to geometric frustration.

While increasing  $U$  universally enhances local moment formation, only the doped systems exhibit a substantial reorganization of spin correlations into anisotropic, compensated textures. These results reinforce the conclusion that charge doping is essential for stabilizing correlation-driven altermagnetic patterns on the frustrated lattice.

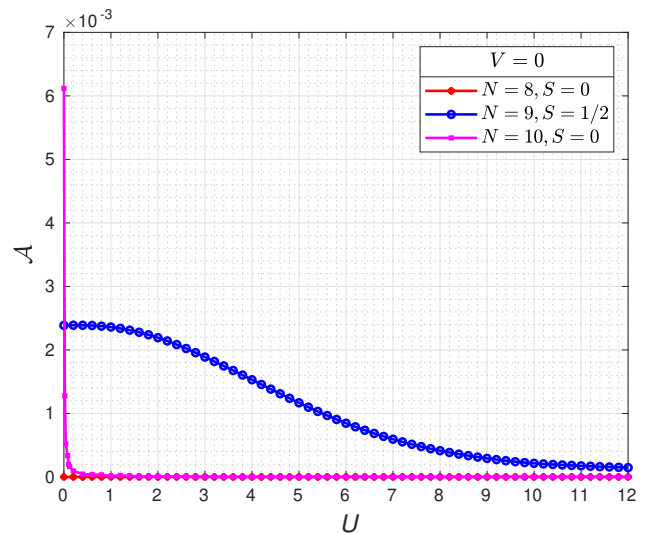


FIG. 5. Anisotropy parameter  $\mathcal{A}$  as a function of on-site interaction  $U$  for the simple Hubbard model ( $V = 0$ ) at fillings  $N = 8, 9, 10$ .

To quantify possible rotational symmetry breaking in the real-space correlation structures, we analyze the anisotropy

parameter  $\mathcal{A}$ , shown in Fig. 5, as a function of the on-site interaction  $U$ . This quantity measures the difference between correlation amplitudes along the lattice  $x$ - and  $y$ -directions and therefore serves as a diagnostic for  $C_4$  symmetry breaking. The half-filled system displays a finite anisotropy at small  $U$ , which gradually decreases as interactions strengthen. The initial enhancement of  $\mathcal{A}$  at weak coupling reflects an imbalance in correlation amplitudes arising from geometric frustration on the odd-site torus. As  $U$  increases and local moments become well defined, the system evolves toward a more isotropic correlation regime, leading to a monotonic suppression of  $\mathcal{A}$ . In the strong-coupling limit, the anisotropy becomes very small, consistent with the effective Heisenberg description in which exchange interactions are uniform along symmetry-related bonds. In contrast, for the doped systems, the anisotropy parameter remains essentially zero across the entire interaction range. In the hole-doped system ( $N = 8$ ),  $\mathcal{A}$  is negligibly small for all  $U$ , indicating that the correlation structure preserves the discrete rotational symmetry of the lattice despite the strong enhancement of  $\langle \Delta_{\text{spin}} \rangle$ . The electron-doped system ( $N = 10$ ) shows a negligible transient spike at very small  $U$ , it rapidly stabilizes to a zero-anisotropy regime, signaling a robust, rotationally symmetric altermagnetic ground state.

Taken together with the average spin-response measure  $\langle \Delta_{\text{spin}} \rangle$  and the spatial heatmaps  $\Omega_{5j}$ , the vanishing anisotropy in the doped sectors, confirms that  $N = 8$  and  $N = 10$  systems support a stable, rotationally symmetric altermagnetic order. In contrast, the finite and decaying anisotropy for  $N = 9$  system highlights the competitive role of geometric frustration, which prevents the formation of a coherent symmetric phase at half-filling.

## B. Extended Hubbard Model

We now turn to investigate the role of NN Coulomb interaction  $V$  at intermediate coupling  $U = 4$  and strong coupling  $U = 10$  in the range  $0 < V \leq U/2$ .

### 1. $U=4$ case

To assess the stability of the interaction-driven magnetic phases against non-local correlations, we examine the average altermagnetic spin-response measure  $\langle \Delta_{\text{spin}} \rangle$  as a function of the NN Coulomb interaction  $V$  at fixed intermediate coupling  $U = 4$ , shown in Fig. 6. For the half-filled system ( $N = 9, S = 1/2$ ),  $\langle \Delta_{\text{spin}} \rangle$  remains consistently low for all  $V$  values, indicating that NN interactions do not alleviate the geometric frustration inherent in the  $3 \times 3$  lattice at half-filling; instead,  $V$  further suppress the already negligible staggered spin correlations. In contrast to the half-filled case, the doped systems ( $N = 8$  and  $N = 10$ , both  $S = 0$ ) maintain significantly higher altermagnetic signatures, though they respond differently to increasing  $V$ . The one-hole-doped ( $N = 8$ ) system exhibits a robust and smooth decrease in  $\langle \Delta_{\text{spin}} \rangle$  with increasing  $V$  suggesting that the altermagnetic state remains the stable ground state throughout this intermediate- $V$  regime. The one-

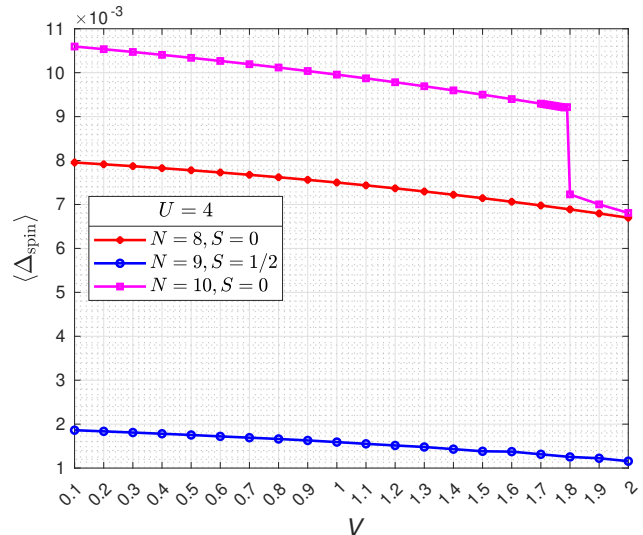


FIG. 6. Average altermagnetic spin-response measure  $\langle \Delta_{\text{spin}} \rangle$  as a function of NN Coulomb interaction  $V$  for the extended Hubbard model at fixed  $U = 4$  on  $3 \times 3$  frustrated square lattice. Results are shown for half-filling ( $N = 9, S = \frac{1}{2}$ ) and for one-hole ( $N = 8, S = 0$ ) and one-electron ( $N = 10, S = 0$ ) doping.

electron-doped ( $N = 10$ ) system initially follows a similar gradual decrease in  $\langle \Delta_{\text{spin}} \rangle$  until reaching a critical threshold at approximately  $V_c \approx 1.8$ . At this point, the system undergoes a sharp, first-order-like drop in the altermagnetic measure. This sudden collapse suggests a rapid reconfiguration of the electronic state, likely driven by  $V$  favoring a competing charge-ordered or non-magnetic phase that becomes energetically more favorable than the altermagnetic manifold at high NN coupling. The comparative analysis reveals that while altermagnetism is generally robust at intermediate  $U$ , it is more susceptible to sudden destabilization by non-local interactions in the electron-doped sector compared to the hole-doped sector.

To complement the analysis of altermagnetic spin correlations, we examine the evolution of the average local moment  $\bar{m}$  as a function of the NN interaction  $V$  at fixed  $U = 4$ , shown in Fig. 7. This quantity allows us to distinguish between changes in the spatial organization of spins and the actual magnitude of local magnetic polarization. At half-filling, the average local moment  $\bar{m}$  decreases gradually as  $V$  increases indicating that NN repulsion does not induce any sharp magnetic transition in this sector. Instead, the monotonic suppression of  $\bar{m}$  reflects the enhanced tendency toward charge redistribution driven by  $V$ , which competes with local moment formation. Comparing  $\bar{m}$  with the observed  $\langle \Delta_{\text{spin}} \rangle$  reveals that the suppression of altermagnetism at half-filling does not arise from an absence of local moments, but rather from the inability of these well-formed moments to overcome frustration and organize into a coherent staggered pattern. The doped sectors exhibit qualitatively different behavior. For the one-hole-doped system ( $N = 8$ ), the local moment decreases steadily with increasing  $V$ . This gradual reduction mirrors the behavior of  $\langle \Delta_{\text{spin}} \rangle$ , indicating that the suppression of the altermagnetic response in this sector arises from a continuous weakening of both the local moment amplitude and the spin

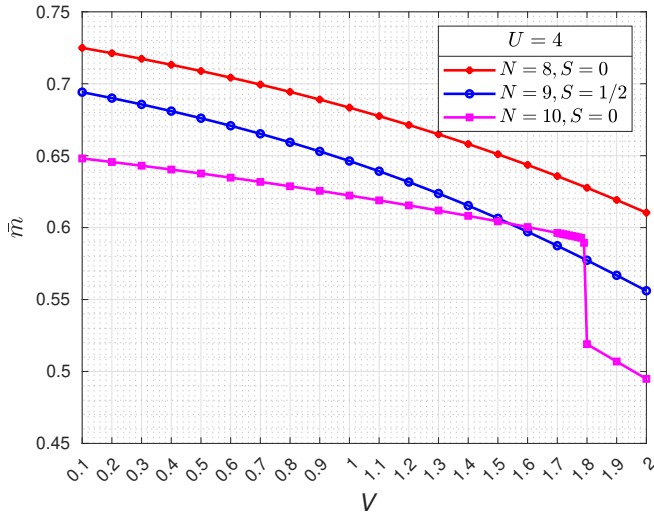


FIG. 7. Average local moment  $\bar{m}$  as a function of NN Coulomb interaction  $V$  for the extended Hubbard model at fixed  $U = 4$  on  $3 \times 3$  frustrated square lattice for half-filling ( $N = 9$ ,  $S = \frac{1}{2}$ ) and for one-hole ( $N = 8$ ,  $S = 0$ ) and one-electron ( $N = 10$ ,  $S = 0$ ) doping.

correlations themselves, rather than from a sudden magnetic collapse. In contrast, the one-electron-doped system ( $N = 10$ ) displays a distinct non-analytic feature. While  $\bar{m}$  initially decreases smoothly for small to intermediate  $V$ , it exhibits a sharp drop near  $V_c \approx 1.8$ , coinciding with the abrupt collapse observed in  $\langle \Delta_{\text{spin}} \rangle$ . This correlated discontinuity signals a rapid reorganization of the ground state. Although the local moment is substantially reduced at the transition, it does not vanish entirely indicating that the instability is not toward a fully non-magnetic state, but rather toward a competing configuration—likely involving enhanced charge correlations—that suppresses the altermagnetic spin correlations while retaining a finite local moment.

To visualize the stability of the altermagnetic state against non-local Coulomb repulsion, we examine real-space heatmaps of the correlation matrix  $\Omega_{5j}$  at intermediate coupling ( $U = 4$ ), shown in Fig. 8. These maps provide a site-resolved perspective on how the NN interaction  $V$  alters the staggered spin-correlation patterns established by  $U$ . At half-filling (middle-row, Fig. 8), the spatial correlations remain consistently fragmented and weak across the entire range of  $V$ . The matrix elements  $\Omega_{5j}$  remain in the  $10^{-3}$  range, and the heatmaps show no discernible  $d$ -wave or staggered symmetry. This spatial disorder confirms that the high local moments observed previously are unable to overcome the geometrical frustration of the  $3 \times 3$  lattice, regardless of the strength of  $V$ . The NN interaction acts only as an additional perturbative scale that fails to organize the frustrated Mott state. In contrast, the doped systems exhibit much stronger, spatially coherent altermagnetic correlation, though their evolution with  $V$  reveals distinct physical regimes. For  $N = 8$  (top-row, Fig. 8), the characteristic anisotropic pattern remains visible across the entire  $V$  range. While the peak intensities at the NN sites gradually diminish as  $V$  increases—consistent

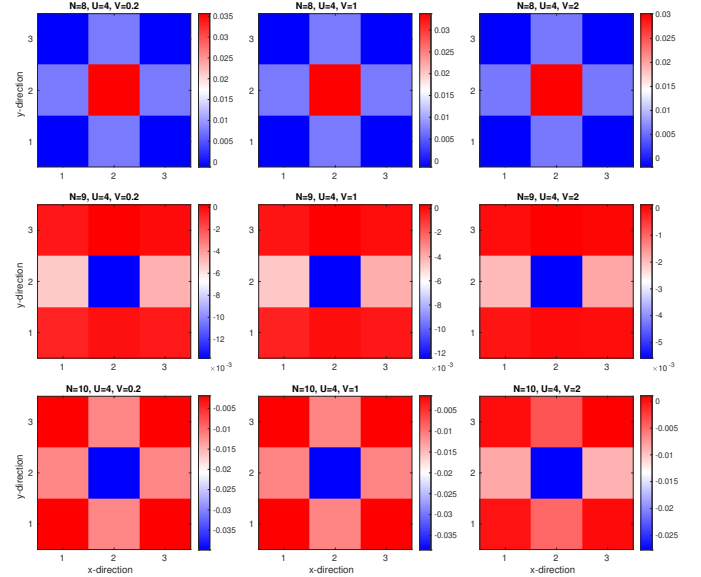


FIG. 8. Real-space heatmaps of the altermagnetic correlation matrix  $\Omega_{5j}$  relative to the central site (site 5) on the  $3 \times 3$  frustrated square lattice of extended Hubbard model at  $U = 4$  for  $N = 8, 9, 10$  at NN Coulomb interaction  $V = 0.2, 1, 2$ .

with the gradual decrease observed in  $\langle \Delta_{\text{spin}} \rangle$ —the fundamental altermagnetic symmetry of the state remains intact. The  $N = 10$  (bottom-row, Fig. 8) sector displays a clear and structured altermagnetic pattern at  $V = 0.2$  and  $V = 1$ . However, at  $V = 2$ , the heatmap undergoes a noticeable transformation. The sharp, staggered intensity observed at lower  $V$  is replaced by a significantly more diffuse and lower-magnitude distribution. This spatial reorganization of the correlation pattern corresponds directly to the first-order-like discontinuity observed in both  $\langle \Delta_{\text{spin}} \rangle$  and  $\bar{m}$ .

In Fig. 9 we examine the anisotropy parameter  $\mathcal{A}$  as a function of NN interaction  $V$ . At half-filling ( $N = 9$ ),  $\mathcal{A}$  assumes finite but small values of order  $10^{-3}$  across the entire range of  $V$ . As  $V$  increases, the anisotropy decreases monotonically indicating that the half-filled system does not undergo any symmetry-breaking instability driven by NN interactions. Instead, the gradual reduction of  $\mathcal{A}$  reflects the overall suppression of magnetic correlations previously observed in  $\langle \Delta_{\text{spin}} \rangle$  and  $\bar{m}$ . The system remains frustrated, nearly isotropic correlated state, with no emergence of coherent directional order. For the hole-doped ( $N = 8$ ) sector,  $\mathcal{A}$  remains essentially zero throughout the explored range of  $V$ . This confirms that the altermagnetic correlation identified in the real-space heatmaps preserves the underlying  $C_4$  lattice symmetry even in the presence of non-local Coulomb repulsion. Combined with the smooth reduction of  $\langle \Delta_{\text{spin}} \rangle$  and  $\bar{m}$ , this result demonstrates that the  $N = 8$  altermagnetic state is structurally robust: NN interactions renormalize the correlation strength but do not induce any directional imbalance. The electron-doped ( $N = 10$ ) sector shows a qualitatively different evolution. For  $V \leq 1.8$ ,  $\mathcal{A}$  remains near zero, indicating a rotationally symmetric altermagnetic texture similar to the hole-doped case. However, at  $V \approx 1.8$ ,  $\mathcal{A}$  exhibits a sharp spike, coin-

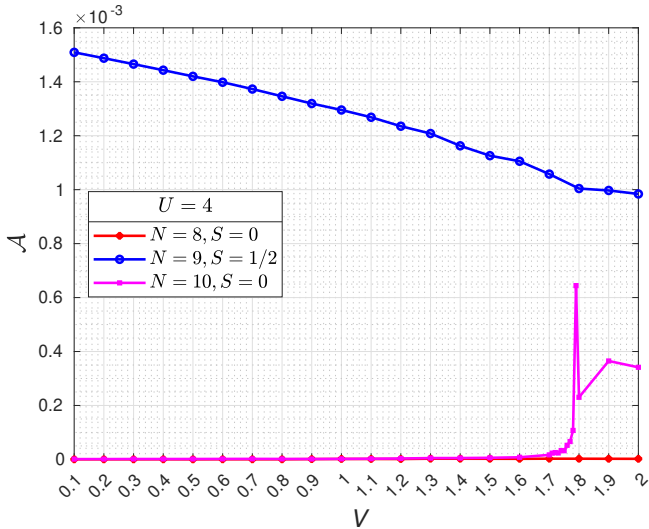


FIG. 9. Anisotropy parameter  $\mathcal{A}$  as a function of NN interaction  $V$  at fixed  $U = 4$ . The  $N = 9$  system maintains rotational symmetry despite frustration. The  $N = 8$  sector shows high stability, while the  $N = 10$  sector exhibits a sharp discontinuity at  $V \approx 1.8$ , marking a symmetry-breaking transition out of the altermagnetic phase as  $V$  approaches  $U/2$ .

ciding with the abrupt suppression of  $\langle \Delta_{\text{spin}} \rangle$  and  $\bar{m}$ . This sudden enhancement of anisotropy signals a rapid reorganization of the ground state. Rather than a simple reduction of magnetic intensity, the system temporarily develops a pronounced directional imbalance as it transitions into a competing correlated configuration at large  $V$ . While finite-size effects prevent a strict thermodynamic classification, the simultaneous discontinuities in multiple observables strongly indicate a first-order-like reconstruction of the electron-doped ground state near  $V \sim U/2$ .

In summary, the extended Hubbard model at  $U = 4$  reveals a rich interplay between on-site and non-local interactions on the frustrated  $3 \times 3$  lattice. While the half-filled system remains a magnetically disordered Mott insulator across all  $V$ , characterized by stable local moments but no long-range correlations, the doped sectors exhibit distinct behaviors. The hole-doped ( $N = 8$ ) system displays a robust altermagnetic state that undergoes continuous suppression with increasing  $V$  while preserving its rotational symmetry. In contrast, the electron-doped ( $N = 10$ ) system experiences a sharp, first-order-like transition at  $V_c \approx 1.8$ , marked by simultaneous discontinuities in the altermagnetic order parameter, local moment and anisotropy. This transition signals a symmetry-breaking reconfiguration into a competing phase—likely involving enhanced charge correlations—that undermine the altermagnetic ground state as  $V$  approaches  $U/2$ . These results establish the doped  $3 \times 3$  lattice as a platform where carrier concentration and non-local interactions critically determine the stability of altermagnetic order.

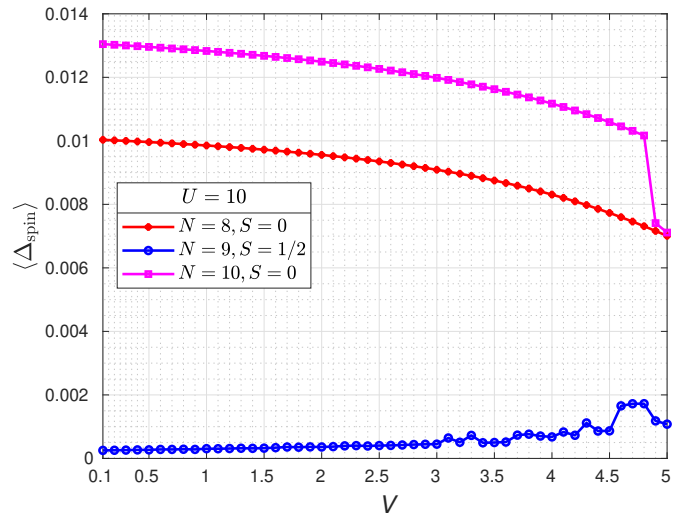


FIG. 10. Average altermagnetic spin-response measure  $\langle \Delta_{\text{spin}} \rangle$  as a function of NN Coulomb interaction  $V$  at  $U = 10$  on  $3 \times 3$  frustrated square lattice for half-filling ( $N = 9$ ,  $S = \frac{1}{2}$ ) and for one-hole ( $N = 8$ ,  $S = 0$ ) and one-electron ( $N = 10$ ,  $S = 0$ ) doping.

## 2. $U=10$ case

We now examine the evolution of the average altermagnetic spin-response measure  $\langle \Delta_{\text{spin}} \rangle$  as a function of NN interaction  $V$  at strong coupling  $U = 10$ , shown in Fig. 10. In this regime, local moments are well developed and the system approaches the Heisenberg limit, allowing us to assess the robustness of carrier-mediated magnetic correlations against non-local Coulomb repulsion. At half-filling ( $N = 9$ ),  $\langle \Delta_{\text{spin}} \rangle$  remains very small across the entire range  $0.1 \leq V \leq 5$ . Although a slight upward trend is visible at large  $V$ , the overall magnitude stays an order of magnitude below that of the doped sectors confirming that even in the strong-coupling limit, geometric frustration on the  $3 \times 3$  torus prevents the formation of a coherent altermagnetic texture. The system remains a frustrated Mott insulator whose spin correlations are insensitive to moderate non-local interactions. In contrast, the doped sectors ( $N = 8$  and  $N = 10$ ) exhibit substantially enhanced altermagnetic responses compared to the intermediate-coupling case. For small and intermediate  $V$ ,  $\langle \Delta_{\text{spin}} \rangle$  decreases gradually and approximately linearly with increasing  $V$ , indicating a smooth renormalization of the carrier-stabilized spin texture. Notably, at  $V \approx 4.9$ , the  $N = 10$  sector show a sharp drop, suggesting that significantly stronger non-local repulsion is required to destabilize the altermagnetic configuration when local moments are fully formed. Overall, the  $U = 10$  results demonstrate that strong on-site repulsion enhances the structural stability of carrier-induced altermagnetic correlations. While NN interaction continuously suppresses the magnitude of the spin-response, the altermagnetic manifold in the doped sectors remains robust over a wide range of  $V$  values, highlighting the stabilizing role of well-localized moments in the strong-coupling regime.

To further probe the stability of the system at strong coupling, we evaluate the average local moment  $\bar{m}$  as a func-

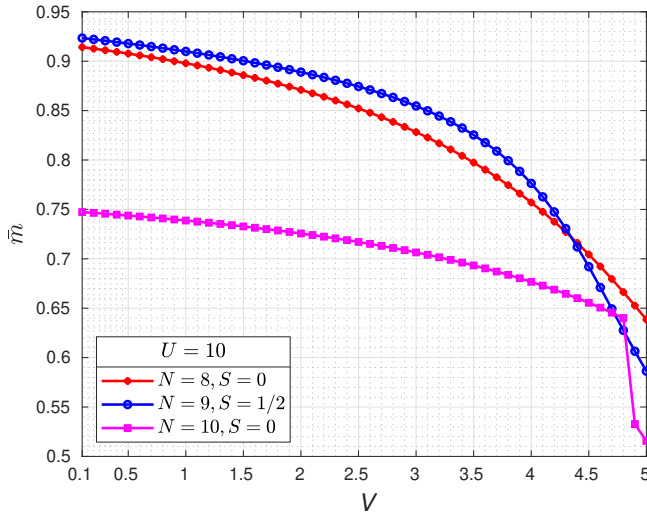


FIG. 11. Average local moment  $\bar{m}$  as a function of NN Coulomb interaction  $V$  at  $U = 10$  for half-filling ( $N = 9$ ,  $S = \frac{1}{2}$ ) and for one-hole ( $N = 8$ ,  $S = 0$ ) and one-electron ( $N = 10$ ,  $S = 0$ ) doping.

tion of the NN interaction  $V$  at fixed  $U = 10$ , shown in Fig. 11. This quantity directly probes the degree of local spin polarization and allows us to assess how robust the magnetic moments remain when non-local Coulomb repulsion is introduced. At half-filling ( $N = 9$ ), the local moment is strongly enhanced compared to the intermediate-coupling case and remains close to saturation for small to moderate  $V$ . Although  $\bar{m}$  decreases gradually as  $V$  increases—particularly for  $V \gtrsim 4$ —its magnitude stays significantly larger than in the  $U = 4$  regime. This behavior reflects the dominant role of the large on-site repulsion, which strongly suppresses double occupancy and stabilizes well-formed local moments. The persistence of large  $\bar{m}$ , despite the absence of a sizable altermagnetic response, confirms that frustration inhibits the spatial organization of spins rather than the formation of local magnetism itself. In the doped sectors ( $N = 8$  and  $N = 10$ ), the average local moment is moderately reduced relative to half-filling due to carrier itinerancy, yet remains substantial throughout the entire  $V$ -range. In particular, the electron-doped system ( $N = 10$ ) exhibits a pronounced, first-order-like drop in  $\bar{m}$  at  $V \approx 4.9$ . Although the local moment remains finite, this abrupt reduction signals a rapid reconstruction of the correlated ground state. Compared to the intermediate-coupling case ( $U = 4$ ), the instability is shifted to significantly larger  $V$ , demonstrating that strong on-site repulsion stabilizes the local magnetic manifold and raises the energy scale required for competing charge-driven configurations to destabilize it.

To obtain a spatially resolved picture of the strong-coupling regime, we examine the real-space heatmaps of the altermagnetic correlation matrix  $\Omega_{5j}$  at fixed  $U = 10$  for  $V = 1, 3, 5$ , shown in Fig. 12. The central site (site 5) is used as the reference to visualize how NN repulsion alters the spin-correlation texture. At half-filling ( $N = 9$ , middle row), the correlations remain extremely small across all values of  $V$ , with magnitudes confined to the  $10^{-3}$ - $10^{-4}$

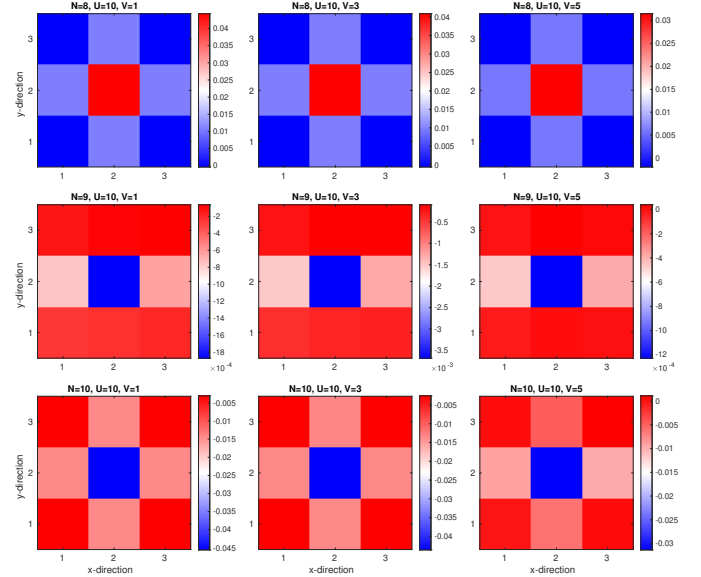


FIG. 12. Real-space heatmaps of the altermagnetic correlation matrix  $\Omega_{5j}$  relative to the central site (site 5) on the  $3 \times 3$  frustrated square lattice at NN Coulomb interaction  $V = 1, 3, 5$  at fixed  $U = 10$  for  $N = 8, 9, 10$ .

range. The spatial pattern appears weak and fragmented, without any coherent anisotropic structure. Increasing  $V$  does not qualitatively reorganize the texture; instead, it merely rescales the already suppressed correlations. This confirms that even in the strong-coupling limit, geometric frustration prevents the formation of a structured altermagnetic configuration at half-filling. The large local moments observed in Fig. 11 therefore remain spatially disordered rather than coherently arranged. In contrast, the doped sectors exhibit robust and well-defined altermagnetic textures. For the hole-doped system ( $N = 8$ , top row), the characteristic cross-like anisotropic pattern persists from  $V = 1$  to  $V = 5$ . Although the overall intensity of the correlations gradually decreases with increasing  $V$ , the spatial structure and relative bond selectivity remain intact. This behavior mirrors the smooth reduction of  $\langle \Delta_{\text{spin}} \rangle$  and  $\bar{m}$ , demonstrating that NN interaction renormalizes the magnitude of correlations without altering their symmetry. The electron-doped system ( $N = 10$ , bottom row) shows a similarly coherent altermagnetic texture at  $V = 1$  and  $V = 3$ . Even at  $V = 5$ , where a sharp drop in the averaged observables was observed, the real-space pattern retains its basic anisotropic character, though with reduced magnitude. Unlike the intermediate-coupling case, no abrupt spatial melting of the texture is visible within this range. Instead, the correlation strengths are uniformly suppressed while the overall structure remains recognizable.

To complete the strong-coupling analysis, we examine the anisotropy parameter  $\mathcal{A}$  as a function of NN interaction  $V$  at fixed  $U = 10$ , shown in Fig. 13. This quantity probes the imbalance between correlations along the two lattice directions and therefore serves as a sensitive indicator of rotational symmetry breaking. At half-filling ( $N = 9$ ),  $\mathcal{A}$  remains very small, of order  $10^{-3}$ , across the entire  $V$ -range. Although a gradual upward trend with

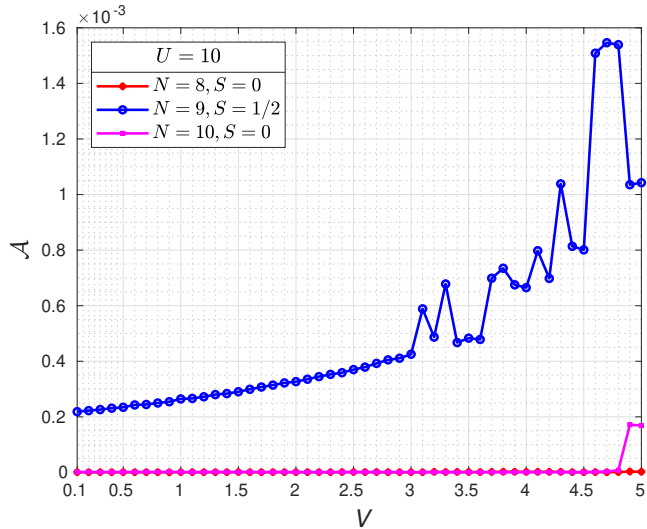


FIG. 13. Anisotropy parameter  $\mathcal{A}$  as a function of NN Coulomb interaction  $V$  at  $U = 10$  for  $N = 8, 9, 10$ .

increasing  $V$  is visible—together with minor fluctuations at larger  $V$ —the magnitude stays extremely small and no sharp discontinuity is observed. This behavior indicates that the frustrated Mott state does not develop any coherent directional order even under strong NN repulsion. The increase in  $\mathcal{A}$  at large  $V$  reflects only a slight redistribution of weak correlations rather than genuine rotational symmetry breaking. In the hole-doped sector ( $N = 8$ ),  $\mathcal{A}$  remains essentially zero throughout the explored range. This confirms that the altermagnetic texture identified in the real-space heatmaps preserves the underlying  $C_4$  lattice symmetry even at strong coupling. The continuous suppression of  $\langle \Delta_{\text{spin}} \rangle$  and  $\bar{m}$  with increasing  $V$  therefore occurs without inducing any directional imbalance. For the electron-doped case ( $N = 10$ ),  $\mathcal{A}$  also remains negligible for most of the  $V$ -range, with only a small enhancement appearing near the largest value  $V \approx 5$ , where a reduction in the averaged observables was previously identified. We observe that, even at this point, the magnitude of  $\mathcal{A}$  remains very small, and no pronounced spike comparable to the intermediate-coupling ( $U = 4$ ) case is observed. This demonstrates that the strong on-site interaction suppresses the symmetry-breaking instability seen at weaker coupling.

In summary, the strong-coupling regime ( $U = 10$ ) is characterized by well-formed and robust local moments that stabilize carrier-induced altermagnetic correlations over a broad range of NN interaction  $V$ . At half-filling, geometric frustration continues to suppress coherent altermagnetic order despite the presence of large local moments, preserving a frustrated Mott state with negligible anisotropy. In contrast, hole and electron doping generate pronounced and spatially structured altermagnetic textures that remain symmetry-preserving and resilient against moderate non-local repulsion. Although increasing  $V$  gradually renormalizes the magnitude of spin correlations—and induces a sharp reconstruction in the electron-doped case at large  $V$ —no genuine rotational symmetry breaking emerges. Overall, strong on-site repulsion enhances the stability of the altermagnetic manifold and shifts competing charge-

driven instabilities to significantly higher energy scales.

#### IV. SUMMARY AND CONCLUSION

In this work, we have performed a many-body investigation of correlation-driven altermagnetism in the simple and extended Hubbard models on the geometrically frustrated  $3 \times 3$  square lattice. Motivated by recent conceptual advances in altermagnetism [27, 30, 57], symmetry classifications [28, 31, 58] and microscopic model studies [59–63], we addressed a central open question: can purely electronic correlations on a symmetric geometrically frustrated lattice give rise to robust altermagnetic order without engineered hopping anisotropy or spin-orbit coupling?

Our results demonstrate that altermagnetic correlations can arise purely from electron-electron interactions on a symmetric geometrically frustrated lattice, without any engineered hopping anisotropy or spin-orbit coupling [60, 64–66]. This identifies a correlation-only pathway to altermagnetism that complements established symmetry-based classifications.

In the simple Hubbard model ( $V = 0$ ), the doped sectors ( $N = 8, 10$ , both with  $S = 0$ ) exhibit a strong enhancement of the altermagnetic spin-response measure with increasing  $U$ , accompanied by clearly structured real-space correlation textures. In contrast, the half-filled system ( $N = 9$ ,  $S = 1/2$ ) shows well-developed local moments but strongly suppressed altermagnetic response due to geometric frustration. This demonstrates that local moment formation alone is insufficient; coherent anisotropic correlation requires carrier-mediated coupling of spins. Our results thus provide fluctuation-driven microscopic support to proposals that altermagnetism can arise as a spontaneous electronic instability [42], extending beyond mean-field or symmetry-engineered constructions [45].

A central finding of this work is the strong spin-sector selectivity of altermagnetic correlations. The robust enhancement of  $\langle \Delta_{\text{spin}} \rangle$  occurs exclusively in the lowest total-spin sectors ( $S = 0$  for doped systems,  $S = 1/2$  for half-filling), highlighting the decisive role of quantum spin fluctuations in stabilizing altermagnetic order. The introduction of mobile charge carriers (holes or electrons) allows the system to lower its kinetic energy by preferentially selecting specific anisotropic hopping paths, which couples to the spin degrees of freedom through the on-site interaction  $U$  and stabilizes the staggered, compensated spin correlations characteristic of altermagnetism [27, 28]. The stronger response for electron doping ( $N = 10$ ) reveals a distinct particle-hole asymmetry in the altermagnetic susceptibility, likely arising from the underlying lattice dispersion and its interplay with geometric frustration.

The inclusion of NN Coulomb repulsion  $V$  in the extended Hubbard model reveals a rich and filling-dependent phase diagram. At intermediate coupling ( $U = 4$ ), the hole-doped ( $N = 8$ ) system exhibits a robust altermagnetic state that undergoes continuous suppression with increasing  $V$  while preserving its  $C_4$  rotational symmetry, as confirmed by the near-zero anisotropy parameter  $\mathcal{A}$ . In striking contrast, the electron-doped ( $N = 10$ ) system undergoes a sharp, first-order-like transition at  $V_c \approx 1.8$ , marked by si-

multaneous discontinuities in  $\langle \Delta_{\text{spin}} \rangle$ ,  $\bar{m}$  and  $\mathcal{A}$ . This correlated collapse signals a rapid reorganization of the ground state into a competing configuration—likely involving enhanced charge correlations—that undermines the altermagnetic order as  $V$  approaches  $U/2$ . The spatial melting of the correlation texture observed in the real-space heatmaps  $\Omega_{5j}$  at  $V = 2$  provides direct microscopic confirmation of this instability.

At strong coupling ( $U = 10$ ), the system enters a regime where well-formed local moments are effectively locked by the large on-site repulsion. The half-filled system remains a frustrated Mott insulator with large moments but negligible altermagnetic order, reinforcing the frustration-dominated physics. The doped sectors exhibit substantially enhanced altermagnetic responses compared to intermediate coupling, with  $\langle \Delta_{\text{spin}} \rangle$  and  $\bar{m}$  showing smooth, monotonic evolution across most of the  $V$  range. Notably, the sharp instability observed in the electron-doped sector at  $U = 4$  is shifted to significantly larger  $V \approx 4.9$  at  $U = 10$ , and even there, the anisotropy parameter  $\mathcal{A}$  remains negligibly small, indicating that strong on-site repulsion suppresses the symmetry-breaking instability seen at weaker coupling. The real-space heatmaps at  $U = 10$  confirm that the altermagnetic texture remains structurally intact even when its magnitude is reduced, demonstrating the protec-

tive role of strong correlations.

Collectively, our results establish a minimal geometrically frustrated lattice as a platform where doping, spin sector and non-local Coulomb interactions jointly determine the emergence and stability of altermagnetic order. Unlike lattice-specific constructions such as modified Lieb geometries [67], the present study demonstrates that correlation-driven altermagnetism can arise on a symmetric geometrically frustrated square lattice purely from many-body effects. Furthermore, the identification of  $V$  as a tunable destabilizing channel suggests possible experimental relevance in correlated materials where screening length or dipolar interactions can be controlled, as well as in ultracold-atom realizations of extended Hubbard model.

In conclusion, this study provides direct many-body evidence that altermagnetism can emerge as a fluctuation-stabilized, correlation-driven phenomenon on a geometrically frustrated lattice, without single-particle anisotropy or spin-orbit coupling. Strong on-site repulsion enhances the robustness of the altermagnetic manifold, while non-local interactions introduce controlled pathways for its reconstruction. These findings broaden the microscopic foundation of altermagnetism and clarify the fundamental role of electronic correlations in stabilizing compensated yet anisotropic spin order.

- 
- [1] E. Dagotto, Correlated electrons in high-temperature superconductors, *Rev. Mod. Phys.* **66**, 763 (1994).
- [2] E. Dagotto, Complexity in strongly correlated electronic systems, *Science* **309**, 257 (2005).
- [3] M. Imada, A. Fujimori, and Y. Tokura, Metal-insulator transitions, *Rev. Mod. Phys.* **70**, 1039 (1998).
- [4] H. Park, K. Haule, and G. Kotliar, Cluster dynamical mean field theory of the mott transition, *Phys. Rev. Lett.* **101**, 186403 (2008).
- [5] M. Chatzieftheriou, S. Biermann, and E. A. Stepanov, Local and nonlocal electronic correlations at the metal-insulator transition in the two-dimensional hubbard model, *Phys. Rev. Lett.* **132**, 236504 (2024).
- [6] M. F. Equbal and M. A. H. Ahsan, Spin-resolved mott crossover and entanglement in the half-filled hubbard model, *Annals of Physics* **488**, 170414 (2026).
- [7] C. C. Tsuei and J. R. Kirtley, Pairing symmetry in cuprate superconductors, *Rev. Mod. Phys.* **72**, 969 (2000).
- [8] E. Fradkin, S. A. Kivelson, and J. M. Tranquada, Colloquium: Theory of intertwined orders in high temperature superconductors, *Rev. Mod. Phys.* **87**, 457 (2015).
- [9] B. Keimer, S. Kivelson, M. Norman, S. Uchida, and J. Zaanen, From quantum matter to high-temperature superconductivity in copper oxides, *Nature* **518**, 179 (2015).
- [10] M. F. Equbal and M. A. H. Ahsan, Binding of holes and competing spin-charge order in simple and extended hubbard model on cylindrical lattice: An exact diagonalization study, arXiv preprint arXiv:2512.10577 (2025).
- [11] L. Savary and L. Balents, Quantum spin liquids: a review, *Reports on Progress in Physics* **80**, 016502 (2016).
- [12] C. Broholm, R. J. Cava, S. A. Kivelson, D. G. Nocera, M. R. Norman, and T. Senthil, Quantum spin liquids, *Science* **367**, eaay0668 (2020), <https://www.science.org/doi/pdf/10.1126/science.aay0668>.
- [13] H.-C. Jiang and S. A. Kivelson, High temperature superconductivity in a lightly doped quantum spin liquid, *Phys. Rev. Lett.* **127**, 097002 (2021).
- [14] S. S. Salunke, M. A. H. Ahsan, R. Nath, A. V. Mahajan, and I. Dasgupta, Electronic structure of spin- $\frac{1}{2}$  heisenberg antiferromagnetic systems:  $\text{Ba}_2\text{Cu}(\text{PO}_4)_2$  and  $\text{Sr}_2\text{Cu}(\text{PO}_4)_2$ , *Phys. Rev. B* **76**, 085104 (2007).
- [15] M. M. Haque and M. A. H. Ahsan,  $\text{Sr}_2\text{Cu}(\text{PO}_4)_2$  and  $\text{Ba}_2\text{Cu}(\text{PO}_4)_2$  as quasi-one-dimensional spin- $\frac{1}{2}$  heisenberg antiferromagnet, *Journal of Magnetism and Magnetic Materials* **402**, 143 (2016).
- [16] J. H. Drewes, L. A. Miller, E. Cocchi, C. F. Chan, N. Wurz, M. Gall, D. Pertot, F. Brennecke, and M. Köhl, Antiferromagnetic correlations in two-dimensional fermionic mott-insulating and metallic phases, *Phys. Rev. Lett.* **118**, 170401 (2017).
- [17] P. Werner, X. Chen, and E. Gull, Ferromagnetic spin correlations in the two-dimensional hubbard model, *Phys. Rev. Res.* **2**, 023037 (2020).
- [18] P. Wrzosek and K. Wohlfeld, Hole in the two-dimensional ising antiferromagnet: Origin of the incoherent spectrum, *Phys. Rev. B* **103**, 035113 (2021).
- [19] J. Hubbard, Electron correlations in narrow energy bands, *Proceedings of the Royal Society A* **276**, 238–257 (1963).
- [20] M. C. Gutzwiller, Effect of correlation on the ferromagnetism of transition metals, *Phys. Rev. Lett.* **10**, 159 (1963).
- [21] J. Kanamori, Electron Correlation and Ferromagnetism of Transition Metals, *Progress of Theoretical Physics* **30**, 275 (1963).
- [22] R. Micnas, J. Ranninger, and S. Robaszkiewicz, Superconductivity in narrow-band systems with local nonretarded attractive interactions, *Rev. Mod. Phys.* **62**, 113 (1990).
- [23] T. Arai, Exchange interaction and heisenberg’s spin hamiltonian, *Phys. Rev.* **126**, 471 (1962).
- [24] M. A. Tusch, Y. H. Szczech, and D. E. Logan, Magnetism in the hubbard model: An effective spin hamiltonian approach, *Phys. Rev. B* **53**, 5505 (1996).

- [25] L. F. Tocchio, A. Montorsi, and F. Becca, Magnetic and spin-liquid phases in the frustrated  $t-t'$  hubbard model on the triangular lattice, *Phys. Rev. B* **102**, 115150 (2020).
- [26] G.-H. Huang and Z. Wu, Magnetic correlations of a doped and frustrated hubbard model: Benchmarking the two-particle self-consistent theory against a quantum simulator, *Phys. Rev. B* **110**, L100406 (2024).
- [27] L. Šmejkal, J. Sinova, and T. Jungwirth, Emerging research landscape of altermagnetism, *Phys. Rev. X* **12**, 040501 (2022).
- [28] L. Šmejkal, J. Sinova, and T. Jungwirth, Beyond conventional ferromagnetism and antiferromagnetism: A phase with nonrelativistic spin and crystal rotation symmetry, *Phys. Rev. X* **12**, 031042 (2022).
- [29] I. Mazin (The PRX Editors), Editorial: Altermagnetism—a new punch line of fundamental magnetism, *Phys. Rev. X* **12**, 040002 (2022).
- [30] T. Jungwirth, R. M. Fernandes, E. Fradkin, A. H. MacDonald, J. Sinova, and L. Šmejkal, Altermagnetism: An unconventional spin-ordered phase of matter, *Newton* **1**, 100162 (2025).
- [31] P. Zhou, X. N. Peng, Y. Z. Hu, B. R. Pan, S. M. Liu, P. B. Lyu, and L. Z. Sun, Transition from antiferromagnets to altermagnets: Symmetry-breaking theory, *Phys. Rev. B* **112**, 144419 (2025).
- [32] G. Sim and J. Knolle, Pair density waves and supercurrent diode effect in altermagnets, *Phys. Rev. B* **112**, L020502 (2025).
- [33] B. Karetta, X. H. Verbeek, R. Jaeschke-Ubiergo, L. Šmejkal, and J. Sinova, Strain-controlled  $g$ - to  $d$ -wave transition in altermagnetic crsb, *Phys. Rev. B* **112**, 094454 (2025).
- [34] D. Chakraborty and A. M. Black-Schaffer, Constraints on superconducting pairing in altermagnets, *Phys. Rev. B* **112**, 014516 (2025).
- [35] Z. Feng, X. Zhou, L. Šmejkal, L. Wu, Z. Zhu, H. Guo, R. González-Hernández, X. Wang, H. Yan, P. Qin, X. Zhang, H. Wu, H. Chen, Z. Meng, L. Liu, Z. Xia, J. Sinova, T. Jungwirth, and Z. Liu, An anomalous hall effect in altermagnetic ruthenium dioxide, *Nature Electronics* **5**, 735 (2022).
- [36] A. Bose, N. J. Schreiber, R. Jain, D.-F. Shao, H. P. Nair, J. Sun, X. S. Zhang, D. A. Muller, E. Y. Tsymlal, D. G. Schlom, and D. C. Ralph, Tilted spin current generated by the collinear antiferromagnet ruthenium dioxide, *Nature Electronics* **5**, 267 (2022).
- [37] T. A. Maier and S. Okamoto, Weak-coupling theory of neutron scattering as a probe of altermagnetism, *Phys. Rev. B* **108**, L100402 (2023).
- [38] L. Bai, W. Feng, S. Liu, L. Šmejkal, Y. Mokrousov, and Y. Yao, Altermagnetism: Exploring new frontiers in magnetism and spintronics, *Advanced Functional Materials* **34**, 2409327 (2024).
- [39] W. Lu, S. Feng, Y. Wang, D. Chen, Z. Lin, X. Liang, S. Liu, W. Feng, K. Yamagami, J. Liu, C. Felser, Q. Wu, and J. Ma, Signature of topological surface bands in altermagnetic weyl semimetal crsb, *Nano Letters* **25**, 7343 (2025).
- [40] C. Song, H. Bai, Z. Zhou, L. Han, H. Reichlova, J. H. Dil, J. Liu, X. Chen, and F. Pan, Altermagnets as a new class of functional materials, *Nature Reviews Materials* **10**, 473 (2025).
- [41] L.-D. Yuan, Z. Wang, J.-W. Luo, E. I. Rashba, and A. Zunger, Giant momentum-dependent spin splitting in centrosymmetric low- $z$  antiferromagnets, *Phys. Rev. B* **102**, 014422 (2020).
- [42] A. Isidori, Altermagnetism arising from a spontaneous electronic instability, *Communications Materials* **5**, 134 (2024).
- [43] S. Giuli, C. Mejuto-Zaera, and M. Capone, Altermagnetism from interaction-driven itinerant magnetism, *Phys. Rev. B* **111**, L020401 (2025).
- [44] S. W. Cheong and F. T. Huang, Altermagnetism classification, *npj Quantum Mater* **10**, 38 (2025).
- [45] V. Leeb, A. Mook, L. Šmejkal, and J. Knolle, Spontaneous formation of altermagnetism from orbital ordering, *Phys. Rev. Lett.* **132**, 236701 (2024).
- [46] S. W. Cheong and F. T. Huang, Altermagnetism with non-collinear spins, *npj Quantum Mater* **9**, 13 (2024).
- [47] M. Alfonso-Moro, V. Guisset, P. David, B. Canals, J. Coraux, and N. Rougemaille, Geometrical frustration, correlated disorder, and emerging order in a corrugated  $c_60$  monolayer, *Phys. Rev. Lett.* **131**, 186201 (2023).
- [48] J. Zhou, G. Quirion, J. A. Quilliam, H. Cao, F. Ye, M. B. Stone, Q. Huang, H. Zhou, J. Cheng, X. Bai, M. Mourigal, Y. Wan, and Z. Dun, Anticollinear order and degeneracy lifting in square lattice antiferromagnet *lasrcro4*, *Phys. Rev. B* **105**, L180411 (2022).
- [49] D. V. Dmitriev and V. Y. Krivnov, Macroscopic degeneracy of the ground state in the frustrated heisenberg diamond chain, *Phys. Rev. B* **111**, 064427 (2025).
- [50] S. Syzranov and A. Ramirez, Eminent phase in frustrated magnets: a challenge to quantum spin liquids, *Nat Commun* **13**, 2993 (2022).
- [51] B.-B. Chen, Z. Chen, S.-S. Gong, D. N. Sheng, W. Li, and A. Weichselbaum, Quantum spin liquid with emergent chiral order in the triangular-lattice hubbard model, *Phys. Rev. B* **106**, 094420 (2022).
- [52] Y. Liu, J. Li, P. Liu, and Q. Liu, Unconventional spin textures emerging from a universal symmetry theory of spin-momentum locking, *npj Quantum Mater* **9**, 69 (2024).
- [53] M. F. Equbal, S. R. Hassan, and M. A. H. Ahsan, Exact diagonalization study of ground state properties and level statistics in simple and extended hubbard lattice cluster, *Physica Scripta* **100**, 035964 (2025).
- [54] M. F. Equbal, S. R. Hassan, and M. A. H. Ahsan, Principal component analysis of competing correlations in quarter-filled hubbard models, *arXiv preprint arXiv:2511.12551* (2025).
- [55] M. A. H. Ahsan and C. R. Sarma, Configuration space truncation scheme for hubbard hamiltonian, *Journal of Chemical Sciences* **106**, 379 (1994).
- [56] C. R. Sarma and M. A. H. Ahsan, Electron correlation studies: Rumer basis approach, *International Journal of Quantum Chemistry* **60**, 147 (1996).
- [57] S. M. Hussain and K. Son, Exploring altermagnetism in ruo2: A review of a new paradigm in spintronics, *Physica B: Condensed Matter* **716**, 417723 (2025).
- [58] S. Zeng and Y.-J. Zhao, Description of two-dimensional altermagnetism: Categorization using spin group theory, *Phys. Rev. B* **110**, 054406 (2024).
- [59] P. A. McClarty and J. G. Rau, Landau theory of altermagnetism, *Phys. Rev. Lett.* **132**, 176702 (2024).
- [60] P. Das, V. Leeb, J. Knolle, and M. Knap, Realizing altermagnetism in fermi-hubbard models with ultracold atoms, *Phys. Rev. Lett.* **132**, 263402 (2024).
- [61] H. Schiff, P. McClarty, J. G. Rau, and J. Romhányi, Collinear altermagnets and their landau theories, *Phys. Rev. Res.* **7**, 033301 (2025).
- [62] P. M. Cónsoli and M. Vojta,  $su(n)$  altermagnetism: Lattice models, magnon modes, and flavor-split bands, *Phys. Rev. Lett.* **134**, 196701 (2025).
- [63] H. Peng, S. Zeng, J.-H. Liao, C.-C. He, X.-B. Yang, and Y.-J. Zhao, Multicomponent altermagnet: A general approach to generating multicomponent

- ment structures with two-dimensional altermagnetism, *Phys. Rev. B* **111**, 195123 (2025).
- [64] S. A. A. Ghorashi and Q. Li, Dynamical generation of higher-order spin-orbit coupling, topology, and persistent spin texture in light-irradiated altermagnets, *Phys. Rev. Lett.* **135**, 236702 (2025).
- [65] Z.-M. Wang, Y. Zhang, S.-B. Zhang, J.-H. Sun, E. Dagotto, D.-H. Xu, and L.-H. Hu, Spin-orbital altermagnetism, *Phys. Rev. Lett.* **135**, 176705 (2025).
- [66] A. T. Costa, J. C. G. Henriques, and J. Fernández-Rossier, Giant spatial anisotropy of magnon Landau damping in altermagnets, *SciPost Phys.* **18**, 125 (2025).
- [67] N. Kaushal and M. Franz, Altermagnetism in modified lieb lattice hubbard model, *Phys. Rev. Lett.* **135**, 156502 (2025).